

UC San Diego

UC San Diego Previously Published Works

Title

Lattice strain effects on the optical properties of MoS₂ nanosheets

Permalink

<https://escholarship.org/uc/item/7f29w4k2>

Journal

Scientific Reports, 4(1)

ISSN

2045-2322

Authors

Yang, Lei
Cui, Xudong
Zhang, Jingyu
et al.

Publication Date

2014

DOI

10.1038/srep05649

Peer reviewed



OPEN

Lattice strain effects on the optical properties of MoS₂ nanosheets

SUBJECT AREAS:

ELECTRICAL AND
ELECTRONIC
ENGINEERING

TWO-DIMENSIONAL MATERIALS

Received
7 February 2014Accepted
24 June 2014Published
10 July 2014Correspondence and
requests for materials
should be addressed to
B.X. (binxiang@ustc.
edu.cn)Lei Yang¹, Xudong Cui², Jingyu Zhang³, Kan Wang², Meng Shen¹, Shuangshuang Zeng¹, Shadi A. Dayeh⁴,
Liang Feng⁵ & Bin Xiang¹

¹Department of Materials Science & Engineering, CAS key Lab of Materials for Energy Conversion, University of Science and Technology of China, Hefei, Anhui, 230026, China, ²Science and Technology on Plasma Physics Laboratory, Research Center of Laser Fusion, CAEP, Sichuan, 621900, China, ³Molecular Foundry, Lawrence Berkeley National Laboratory, 1 Cyclotron Rd, Berkeley, CA 94720, USA, ⁴Department of Electrical and Computer Engineering, University of California San Diego, La Jolla, CA, 92093, USA, ⁵Department of Electrical Engineering, The State University of New York at Buffalo, Buffalo, NY, 14228, USA.

“Strain engineering” in functional materials has been widely explored to tailor the physical properties of electronic materials and improve their electrical and/or optical properties. Here, we exploit both in plane and out of plane uniaxial tensile strains in MoS₂ to modulate its band gap and engineer its optical properties. We utilize X-ray diffraction and cross-sectional transmission electron microscopy to quantify the strains in the as-synthesized MoS₂ nanosheets and apply measured shifts of Raman-active modes to confirm lattice strain modification of both the out-of-plane and in-plane phonon vibrations of the MoS₂ nanosheets. The induced band gap evolution due to in-plane and out-of-plane tensile stresses is validated by photoluminescence (PL) measurements, promising a potential route for unprecedented manipulation of the physical, electrical and optical properties of MoS₂.

Transition metal dichalcogenides, such as MoS₂, have attracted considerable attention for their potential advantages in catalysis^{1–4}, transistors^{5–7}, batteries^{8,9}, gas sensors¹⁰, photodetectors¹¹, and other optoelectronic devices¹². Bulk crystals of MoS₂, with an indirect band-gap of 1.3 eV, possess strong intra-layer sulfur-metal covalent bonds where the metal atoms are sandwiched by sulfur atoms but their interlayer stacking is weakly supported by van der Waals forces¹³. Single-layer MoS₂, however, shows distinctly promising semiconductive properties with a direct band-gap of 1.9 eV¹⁴, exhibiting strong photoluminescence¹⁵, high in-plane carrier mobility (200–500 cm²/V·s)¹⁶ and robust mechanical properties¹⁷. Interestingly, such indirect-to-direct band gap transition from the bulk form to the monolayer form due to quantum confinement leads to strong enhancement of photoluminescence (PL) from MoS₂¹⁴, therefore creating a series of promising applications for two-dimensional (2D) material-based optoelectronics^{11,18}. This is afforded through the large yield of monolayer MoS₂ synthesis by chemical vapor deposition (CVD) that has been utilized to build up atomically thin optoelectronic devices^{19,20}. Moreover, it would be desirable to achieve a wider optical spectral response if the band gap of layered MoS₂ can be systematically controlled. “Strain engineering” has been shown to exert a profound impact on the properties of MoS₂^{21–23}. Since MoS₂ can endure large strains before breaking^{24,25}, tuning the MoS₂ band gap by lattice strain becomes an important strategy to enhance the performance of nanodevices made from MoS₂. In this work, we systematically investigated the effects of in-plane and out-of-plane tensile strains of MoS₂ nanosheets and explored the associated strain engineering of their band gap. The lattice strains in as-synthesized MoS₂ nanosheets were quantified using the X-ray diffraction (XRD), cross-sectional high-resolution transmission electron microscope (TEM) analysis and Raman spectroscopy. The band gap evolution of MoS₂ nanosheets induced by the strains was validated by PL measurements, which is qualitatively consistent with our theoretical analysis using density functional theory (DFT) calculations.

The phase of MoS₂ nanosheets synthesized using a hydrothermal method (Fig. S1) is confirmed to be a hexagonal structure of MoS₂ with space group P 63/mmc as indexed by JCPDF card number 37-1492. Particularly, the peak of (002) plane (c-axis) shifts to a smaller angle while the peak of (100) plane shifts to a larger angle, indicating that there is an expansion along [001] direction and in-plane compression in the as-synthesized MoS₂ nanosheets. The atomic plane spacing in the MoS₂ nanosheets can be calculated from the XRD pattern using the Bragg equation²⁶:

$$2d\sin\theta = n\lambda \quad (1)$$



where d is the atomic plane spacing, θ is the Bragg scattering angle, n is the diffraction order and λ is the wavelength of incident X-ray. Using Equation (1), the XRD result showed a calculated interlayer spacing ((002) Miller indices spacing) of 6.1924 Å for the as-synthesized MoS₂ nanosheets that is larger compared to that of bulk MoS₂ (6.1554 Å)²⁷. The observed difference in the (002) plane spacing causes a uniaxial tensile strain along [001] direction in the as-synthesized MoS₂ nanosheets. By tuning the PH value in the reaction solution, the lattice strains in as-synthesized MoS₂ nanosheets could be modified (Supporting Information, Figure S2). The morphology of the as-synthesized MoS₂ nanosheets was characterized by scanning electron microscopy (SEM), showing that the 2D MoS₂ nanosheets rolled up and thus formed a three-dimensional (3D) network with highly curved walls (Figure S3). From the high resolution TEM (HRTEM) image of the basal plane of the as-synthesized MoS₂ nanosheets shown in Figure 1b, we can see hexagonal rings of alternative molybdenum and sulphur atoms in each unit, meaning that the MoS₂ nanosheets are of high quality with defect-free atomic lattices. The corresponding zone axis is along [001] direction as confirmed using the fast Fourier transform (FFT) shown in the inset of Figure 1b. The marked (100) and (010) atomic plane distances (~2.7 Å) are both smaller (~1%) than their corresponding lattice spacing in bulk MoS₂²⁸, indicating an in-plane biaxial compressive strain in the basal plane. We also applied HRTEM to image the cross-section of the MoS₂ nanosheets (Figure 1c). Typical nanosheets con-

sist of 5, 6, 9, and 10 layers, from which the interlayer spacing can be measured accordingly (Supporting Information). The average of the measured interlayer spacing is 6.2282 Å in the as-synthesized MoS₂ nanosheets (Figure 1d), which is about 1% larger than the bulk interlayer spacing (6.1554 Å) indicating an out-of-plane uniaxial tensile strain along [001] direction, consistent with the XRD results discussed above. These results confirm that the as-synthesized MoS₂ nanosheets contain an out-of-plane uniaxial tensile strain and an in-plane biaxial compressive strain as depicted in Figure 1e.

Figure 2a shows Raman spectra of as-synthesized MoS₂ nanosheets (grown from pH = 7 and pH < 7 solutions, respectively), strain-partially released MoS₂ nanosheets (grown at pH < 7 and transferred by solution method to SiO₂/Si substrate, see supporting information), bulk MoS₂ (SPI Supplies) and monolayer MoS₂ (CVD growth on SiO₂/Si substrate). Compared with bulk MoS₂, there is a red shift of A_{1g} mode observed in the monolayer MoS₂ with $\Delta\omega = 3 \text{ cm}^{-1}$, and for E_{2g}¹ mode, a blue shift ($\Delta\omega = 2 \text{ cm}^{-1}$) exists in the monolayer MoS₂. In the Raman spectra of MoS₂ nanosheets grown from pH = 7 solution and PH < 7 solution, only red shifts for both E_{2g}¹ and A_{1g} modes were observed, compared to bulk MoS₂. Compared to as-synthesized MoS₂ nanosheets, blue shifts of both E_{2g}¹ and A_{1g} modes in the strain-released MoS₂ nanosheets were observed. Figure 2b shows the frequencies of E_{2g}¹ and A_{1g} modes of MoS₂ nanosheets extracted from Figure 2a. The largest red shifts of both

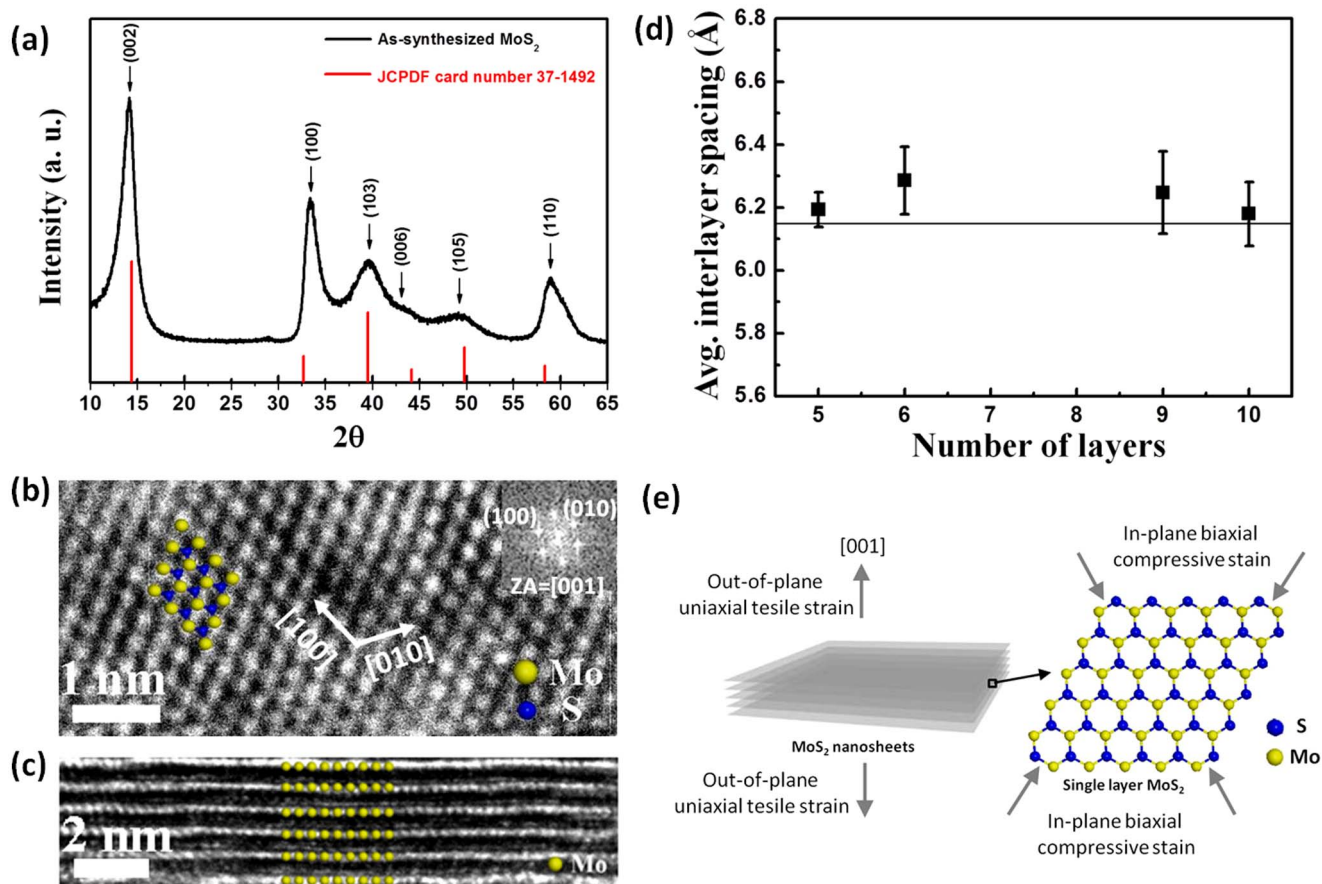


Figure 1 | (a) XRD pattern of MoS₂ nanosheets grown from PH < 7 solution with the line indexed by JCPDF card number 37-1492. (b) HRTEM image of the basal plane of MoS₂ nanosheets grown from PH < 7 solution. Atomic lattice is illustrated by the hexagonal rings of alternating molybdenum and sulphur atomic sites in each unit as illustrated by the cartoon color spheres. The inset shows the corresponding fast Fourier transform (FFT) with a zone axis of [001]. (c) Cross-section HRTEM images of the MoS₂ nanosheets grown from PH < 7 solution. Each layer is denoted by the yellow spheres representing the Mo atoms. The direction of the cross-section HRTEM is along [001]. (d) The average of measured interlayer spacing from HRTEM pictures for different MoS₂ nanosheets consisting of (a) 5, (b) 6, (c) 9 and (d) 10 layers, respectively. The solid line represents the bulk interlayer spacing. (e) Diagram of in-plane biaxial compressive strain and out-of-plane tensile strain in the as-synthesized MoS₂ nanosheets grown from PH < 7 solution.

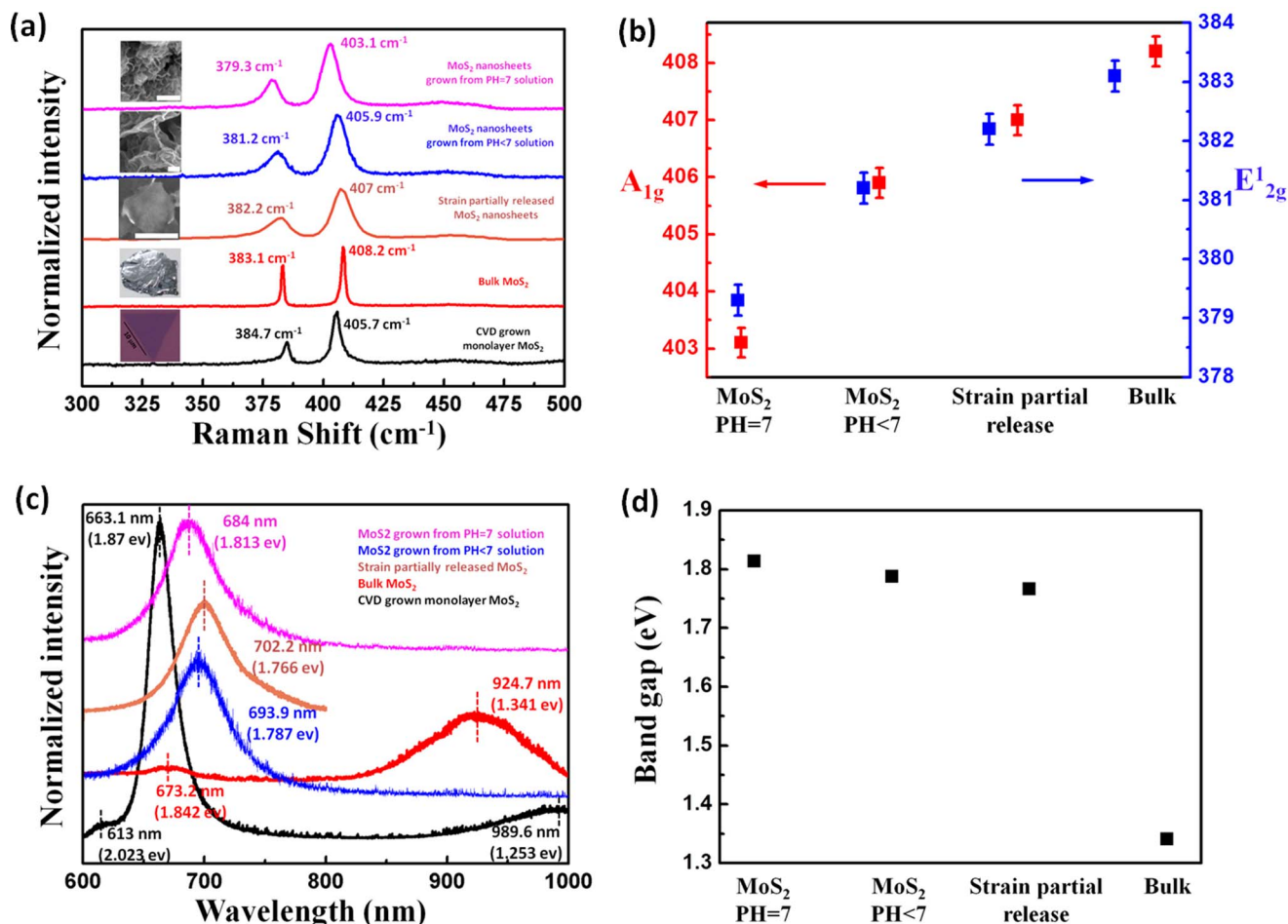


Figure 2 | (a) Raman spectra of as-synthesized MoS₂ nanosheets including grown from pH = 7 (in pink) and pH < 7 (in blue) solution, strain-partially-released MoS₂ nanosheets (in gray), bulk MoS₂ (SPI Supplies) (in red) and monolayer MoS₂ (CVD growth on SiO₂/Si substrate) (in black). The inset images near each spectra correspond to their sample morphologies. Scale bar is 300 nm. (b) The frequencies of E_{2g}¹ and A_{1g} modes extracted from (a). The Raman peak shift error bar indicates the spectrometer resolution. (c) PL spectra of as-synthesized MoS₂ nanosheets (grown from pH = 7 and pH < 7 solution), strain-partially-released MoS₂ nanosheets, bulk MoS₂ (SPI Supplies) and monolayer MoS₂ (CVD growth on SiO₂/Si substrate). (d) The band-gap shifts induced by different lattice strains in MoS₂.

E_{2g}¹ and A_{1g} modes are observed in the MoS₂ nanosheets grown from pH = 7 solution. The strain-caused band-gap shift was also validated as shown in Figure 2c where PL spectra are plotted for bulk MoS₂, monolayer MoS₂, strain-partially released MoS₂ nanosheets and as-synthesized MoS₂ nanosheets. From the PL spectra of the as-synthesized MoS₂ nanosheets, two peaks at 693.9 nm (1.787 eV) (in blue) and 684 nm (1.813 eV) (in pink) were clearly observed, corresponding to a direct transition between the top valence band K point and the bottom conduction K points in the Brillouin zone¹⁴. In comparison with MoS₂ nanosheets grown from pH < 7 solution, a blue shift (26 meV) of the direct band transition was observed in MoS₂ nanosheets grown from pH = 7 solution synthesized MoS₂ nanosheets, while a red shift (21 meV) of the direct band transition was observed in the strain-partially released MoS₂ nanosheets. In monolayer MoS₂, most of the excited electrons and holes recombine with each other through direct band-to-band transition at the K point in the Brillouin zone, leading to strong photoluminescence near 1.87 eV. A weak feature was also observed at 613 nm (2.023 eV) as noted) due to direct-gap hot luminescence¹⁴. For bulk MoS₂, an indirect band gap transition at 924.7 nm (1.341 eV) was observed, which is a transition between the top valence band Γ point and the bottom conduction band halfway between Γ and K points in the Brillouin zone²⁹. The band-gap shifts due to different strain

effects in MoS₂ that were extracted from Figure 2c are shown in Figure 2d.

To further illustrate the band-gap modulation by strain, we investigated the influence of in-plane uniaxial tensile strain on the phonon spectra and the band gap of exfoliated MoS₂ nanosheets. The exfoliated MoS₂ nanosheets were transferred onto a flexible substrate (details in Supporting Information). The solidification process for the polydimethylsiloxane (PDMS) flexible substrate caused the exfoliated MoS₂ nanosheets to strongly adhere to the surface of PDMS (Figure S7). Upon bending the PDMS substrate, an in-plane uniaxial tensile strain is exerted at the top-most plane containing the exfoliated MoS₂ nanosheets. As shown in Figure 3a, the applied strain significantly causes blue shifts in A_{1g} and E_{2g}¹ modes of the exfoliated MoS₂ nanosheets. Assuming that the bending induced strain is entirely transferred to exfoliated MoS₂ nanosheets, we estimated the in plane uniaxial tensile strain ϵ existing in the exfoliated MoS₂ nanosheets by calculating the ratio of the PDMS substrate thickness d to twice the radius of the curvature R as $\epsilon = d/2R$ ³⁰. Figure 3b shows the frequencies of E_{2g}¹ and A_{1g} modes of the exfoliated MoS₂ nanosheets with different local strains extracted from Figure 3a. In Figure 3c prior to bending the PDMS substrate, the exfoliated MoS₂ nanosheets exhibit a PL peak at 880.1 nm (1.409 eV), which is similar to the indirect band transition in bulk MoS₂. We also observed

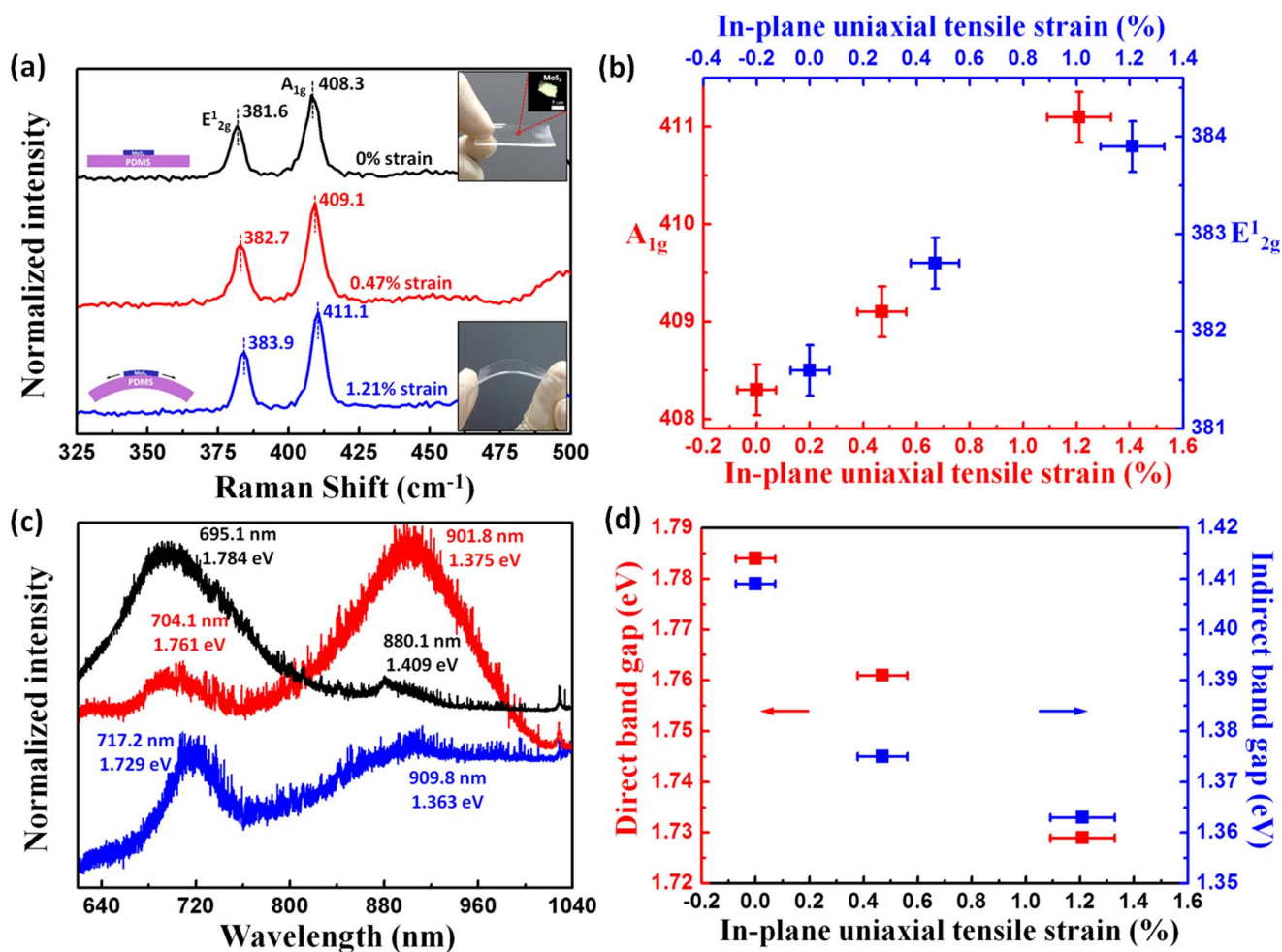


Figure 3 | (a) Raman spectra of the exfoliated MoS₂ nanosheets on PDMS flexible substrate. The insets in (a) show the schematic illustrations of the exfoliated MoS₂ nanosheets on flexible substrate undergoing strain effect. The in-plane uniaxial tensile strain was introduced by bending the PDMS flexible substrate. (b) The frequencies of E_{2g}¹ and A_{1g} modes extracted from (a). The Raman peak shift error bar indicates the spectrometer resolution. (c) The PL spectra of exfoliated MoS₂ nanosheets with 0% (in black), 0.47% (in red), 1.21% (in blue) in-plane uniaxial tensile strain. (d) The PL peaks of exfoliated MoS₂ nanosheets on flexible substrate extracted from (c). The band-gap is decreases by an increase of in-plane uniaxial tensile strain.

another direct band transition PL peak at 695.1 nm (1.784 eV), corresponding to the same direct band-to-band transition as observed in as-synthesized MoS₂ nanosheets. With the in-plane uniaxial tensile strain, red shifts of direct band-to-band transition and indirect band transition are observed by bending the PMDS substrate. Figure 3d shows the PL peaks of the exfoliated MoS₂ nanosheets with different local strains extracted from Figure 3c.

MoS₂ consists of weak bonds between different S-Mo-S layers as illustrated in the stacked structure of Figure 4a. Each layer is electrically neutral, such that nature of the forces between adjacent layers is van der Waals' type³¹. The van der Waals forces between S atoms in adjacent layers dominates the interlayer forces. Figure 4b shows atomic displacements of the four Raman-active modes. In the out-of-plane A_{1g} mode, the restoring force is primarily due to interlayer van der Waals interaction³². With increasing the number of layers, the additional "spring" between S atoms in neighboring layers enhances the restoring force, resulting in an increase of the A_{1g} mode frequency. The in-plane E_{2g}¹ mode is a symmetric mode, which vibrates out of phase as sketched in Figure 4b. The presence of the interlayer interactions can also increase the effective restoring force acting on the basal plane atoms^{31–33}. It has been demonstrated that in bulk graphite, this kind of inter-layer interactions affect the intra-layer bonding and stiffen the in-plane lattice vibrations³⁴. Similarly, with an increase of number of layers in MoS₂ there is an increase in

the frequency of the in-plane E_{2g}¹ mode. Compared to the Raman spectrum of bulk MoS₂, red shifts are observed for both A_{1g} and E_{2g}¹ modes of the as-synthesized MoS₂ nanosheets. As characterized above, there is a uniaxial tensile strain along [001] direction in the as-synthesized MoS₂ nanosheets grown from PH < 7 solution. The out of plane uniaxial tensile strain weakens the interlayer interactions, leading to a decrease in frequencies of both A_{1g} and E_{2g}¹ modes. The inset images in Figure 2a show that the average pore size of 3D MoS₂ networks grown from PH = 7 solution is ~100 nm, smaller than in 3D MoS₂ networks grown from PH < 7 solution. In terms of lattice strain, the difference in the curvature causes a larger strain effect in MoS₂ nanosheets grown from PH = 7 solution as supported by XRD (details in Supporting Information) and the red shifts of both A_{1g} and E_{2g}¹ modes observed in the Raman spectra, compared to that of MoS₂ nanosheets grown from PH < 7 solution. During the sonication process, the 3D networks can be cracked to smaller sheets of strain-released MoS₂ as indicated in the inset of Figure 2a, causing blue shifts of A_{1g} and E_{2g}¹ modes compared to as-synthesized MoS₂ nanosheets. However, mild red shifts (1 cm⁻¹) of both A_{1g} and E_{2g}¹ modes were still observed in strain-partially released MoS₂ nanosheets, in contrast to bulk MoS₂, due to residual strains in these discontinuous nanosheets. This residual strain resulted from the small curvatures observed in the sonicated MoS₂ nanosheets with a

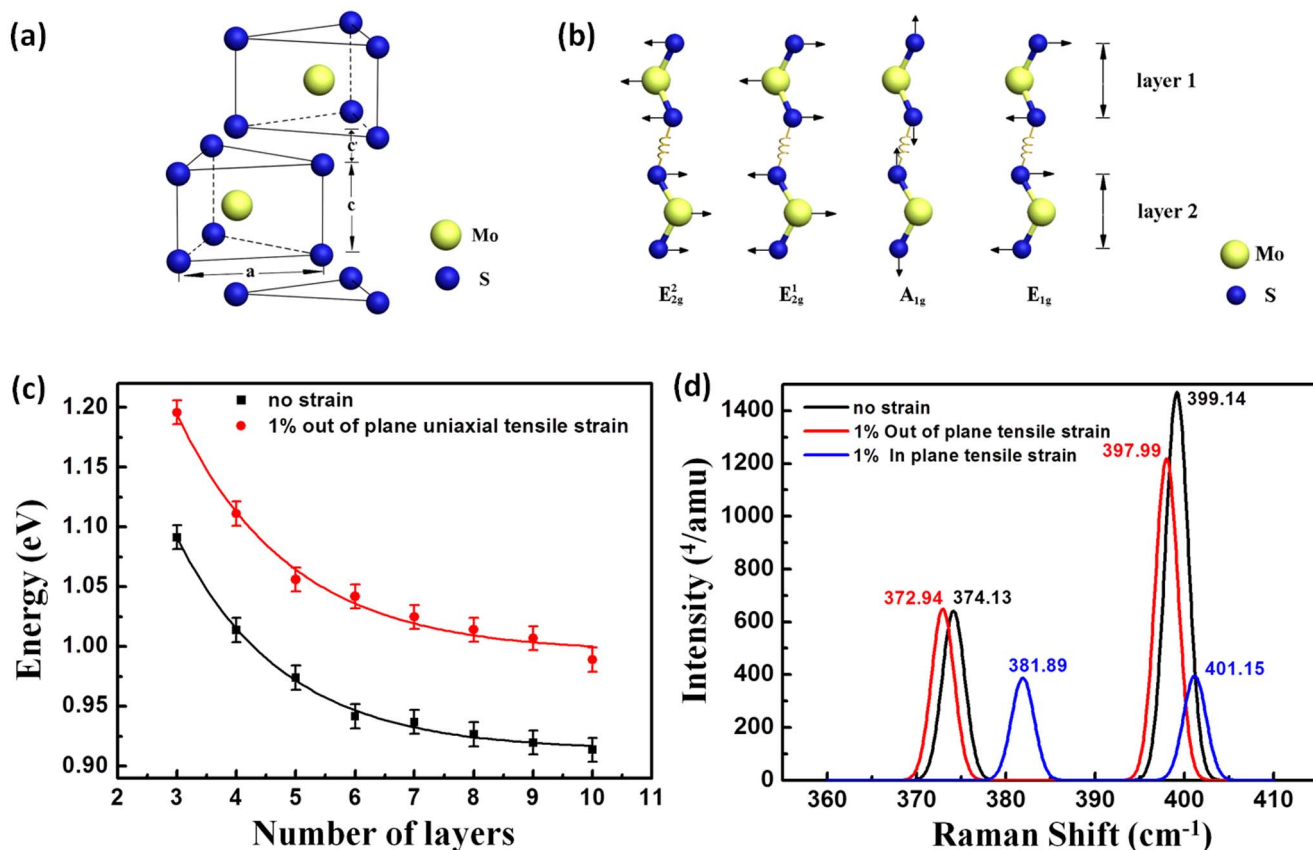


Figure 4 | (a) Crystal structure of hexagonal MoS₂, with strong intra-layer sulfur-metal covalent bonds and weak inter-layer van der Waals stacking. (b) Illustration of the atomic displacements of the four Raman-active modes. (c) The calculated band-gap energies for MoS₂ nanosheets with a different number of layers modulated with 1% out-of-plane tensile strain. (d) The simulated Raman scattering of bulk MoS₂ with the effect of 1% out of plane tensile strain and 1% in-plane tensile strain.

morphology similar to broken-bamboos (Figure S8, Supporting Information). Note that the increase in frequency of the A_{1g} mode from the monolayer to the bulk MoS₂ is 3 cm⁻¹. One might expect that the additional interlayer van der Waals interactions should raise the frequency of E_{2g}¹ mode with an increase of number of layers. However, according to our experimental results shown in Figure 2a, the E_{2g}¹ mode in bulk MoS₂ has a lower frequency (~2 cm⁻¹) than in monolayer MoS₂. This frequency decrease of the E_{2g}¹ mode is possibly due to the long range Coulomb interactions^{32,35} from the coupled dipoles induced from Mo-S bonds. The Coulomb interactions tend to decrease the frequencies of both E_{2g}¹ and E_{1u} (TO) modes^{32,35}. An increase in the number of layers leads to a stronger long-range Coulomb forces and stronger interlayer interactions that are competitive with each other. In few-layer MoS₂ samples, these Coulomb forces are larger than the total forces arising from the interlayer interactions³⁵, while in thicker layered samples, the interlayer interactions become stronger and surpass the Coulomb interactions. In monolayer or few layered samples, the Coulomb interactions dominate the Raman peak shifts. In this case, an in-plane tensile strain effect can lead to a red shift in Raman peaks as reported by Conley et al²¹, resulting from the increase of the Coulomb interactions. While in the thicker layered samples, the interlayer interactions become dominated for the shift of Raman-active mode frequencies. When the number of layers reaches up to 6, the layered sample retains bulk-like behavior and there is no continuous frequency decrease in the observed E_{2g}¹ mode^{14,34}. In our synthesized MoS₂ nanosheets, the Coulomb interactions are smaller than the interlayer interactions. Therefore, undergoing out of plane uniaxial tensile strain, the shifts in frequencies of A_{1g} and E_{2g}¹ modes are

consistent with the classical model of coupled harmonic oscillators³³. In addition, the larger in-plane tensile strain gives rise to larger blue shifts of both E_{2g}¹ and A_{1g} modes as demonstrated in Figure 3a and 3b. The in-plane uniaxial tensile strain can enhance the interlayer interactions in the exfoliated MoS₂ nanosheets, leading to stronger in-plane and out-of-plane effective restoring forces acting on the atoms^{31,32}. Therefore, higher frequencies of A_{1g} and E_{2g}¹ modes are observed in the exfoliated MoS₂ nanosheets with an in-plane uniaxial tensile strain.

It has been established that the energy states of the valence band and conduction band mainly originate from the 3p orbital of S atoms and 4d orbital of Mo atoms³⁶. The interatomic distance change between the Mo and S atoms due to the strain effect can lead to a different superposition of those atomic orbitals. The variations in the overlap between the 3p_z orbital of S and 4d_{z²} orbital of Mo cause shifts in the energy states of the valence band and conduction band³⁶. The presence of the lattice strains therefore modifies the overlap between the S orbital and the Mo orbital, which results in an energy shift in the band gap. In the presence of in-plane uniaxial tensile strain, the direct band gap is tailored by a rate of ~35 meV per 1%, while the indirect band gap is less sensitive to this tensile strain (Figure 3d). The strain is employed to tailor the band-gap by modifying the curvature of the bands, reflecting in a change in the effective masses of electrons and holes³⁷. For MoS₂, the location shift of conduction band extremum generally occurs for much smaller strain than the location shift of the valence band extremum³⁷. Therefore, the strain-induced change in the effective mass of the electron in the conduction band extremum halfway between Γ and K points in the Brillouin zone can reflect the indirect band-gap evolution of MoS₂. As subjected to in-plane uniaxial tensile strain, the effective mass of



electrons in the conduction band extremum halfway between Γ and K points exhibits a slow change with this tensile strain³⁷. This elucidates that the MoS₂ indirect band-gap is less sensitive to in-plane uniaxial tensile strain. However, the effective mass of electrons at the bottom conduction band at K point decreases monotonically by increasing in-plane tensile strain. Therefore, the tunability of the indirect band gap is much smaller than that of the direct band gap in MoS₂ nanosheets by in-plane uniaxial tensile strain.

The evolution of the band gap of the as-synthesized MoS₂ with the number of layers varied as 5, 6, 9, and 10 is also numerically analyzed with the influence of 1% lattice strain as shown in Figure 4c. The calculated band gap tunability by strain is ~ 85 meV per 1% strain. The deviation between the experimental and numerical results is because the strain in the MoS₂ nanosheets is only partially released after the sonication process. Note that the calculated direct band gap value is smaller compared to the results in the PL spectrum. This is mainly due to that the standard exchange-correlation functions of the generalized gradient approximation (GGA) are used in the calculations, by which we usually obtain underestimated results for band-gap energies^{33,38}. However, the band-gap computation indicates that the existence of the out-of-plane uniaxial tensile strain enhances the band gap of the MoS₂, consistent with the experimental results. The simulated Raman scattering (Figure 4d) shows red shifts of Raman-active modes (A_{1g} and E_{2g}^1) with a 1% out of plane tensile strain and blue shifts of Raman-active modes (A_{1g} and E_{2g}^1) with a 1% in-plane tensile strain, which is also consistent with our experimental results. The decrease in PL intensity and peak broadening in as-synthesized MoS₂ nanosheets (Figure 2c) could be due to the exponential enhancement in non-radiative electron–hole recombination processes, reducing the probability of radiative transition³⁹.

In summary, we have experimentally demonstrated the lattice strain effects on the evolution of the band gap in as synthesized and mechanically exfoliated MoS₂ nanosheets. Concurrent studies of X-ray diffraction, cross-sectional high-resolution transmission electron microscopy analysis and Raman spectroscopy reveal the correlation between the structures of the MoS₂ nanosheets and their optical properties. The out-of-plane uniaxial tensile strain gives rise to a blue shift of MoS₂ band-gap whereas the in-plane uniaxial tensile strain results in a red shift of its band-gap. Our results suggest that manipulating the lattice strain by synthetic or mechanical means provides an efficient approach to engineer the band structure of MoS₂.

1. Voiry, D. *et al.* Conducting MoS₂ nanosheets as catalysts for hydrogen evolution reaction. *Nano Lett.* **13**, 6222–6227 (2013).
2. Ataca, C. & Ciraci, S. Dissociation of H₂O at the vacancies of single-layer MoS₂. *Phys. Rev. B* DOI: 10.1103/PhysRevB.85.195410 (2012).
3. Kibsgaard, J., Chen, Z., Reinecke, B. N. & Jaramillo, T. F. Engineering the surface structure of MoS₂ to preferentially expose active edge sites for electrocatalysis. *Nat. Mater.* **11**, 963–969 (2012).
4. Zong, X. *et al.* Enhancement of photocatalytic H₂ evolution on CdS by loading MoS₂ as cocatalyst under visible light irradiation. *J. Am. Chem. Soc.* **130**, 7176–7177 (2008).
5. Radisavljevic, B., Radenovic, A., Brivio, J., Giacometti, V. & Kis, A. Single-layer MoS₂ transistors. *Nat. Nanotech.* **6**, 147–150 (2011).
6. Radisavljevic, B., Whitwick, M. B. & Kis, A. Integrated circuits and logic operations based on single-layer MoS₂. *ACS Nano* **5**, 9934–9938 (2011).
7. Nam, H. *et al.* MoS₂ transistors fabricated via plasma-assisted nanoprining of few-layer MoS₂ flakes into large-area arrays. *ACS Nano* **7**, 5870–5881 (2013).
8. Zhou, G. *et al.* A graphene–pure-sulfur sandwich structure for ultrafast, long-life lithium–sulfur batteries. *Adv. Mater.* **26**, 625–631 (2014).
9. Cao, X. *et al.* Preparation of MoS₂-coated three-dimensional graphene networks for high-performance anode material in lithium-ion batteries. *Small* **9**, 3433–3438 (2013).
10. Late, D. J. *et al.* Sensing behavior of atomically thin-layered MoS₂ transistors. *ACS Nano* **7**, 4879–4891 (2013).
11. Lopez-Sanchez, O., Lembke, D., Kayci, M., Radenovic, A. & Kis, A. Ultrasensitive photodetectors based on monolayer MoS₂. *Nat. Nanotech.* **8**, 497–501 (2013).

12. Wang, Q. H., Kalantar-Zadeh, K., Kis, A., Coleman, J. N. & Strano, M. S. Electronics and optoelectronics of two-dimensional transition metal dichalcogenides. *Nat. Nanotech.* **7**, 699–712 (2012).
13. Kam, K. K. & Parkin, B. A. Detailed photocurrent spectroscopy of the semiconducting group transition metal dichalcogenides. *J. Phys. Chem.* **86**, 463–467 (1982).
14. Mak, K. F., Lee, C., Hone, J., Shan, J. & Heinz, T. F. Atomically thin MoS₂: a new direct-gap semiconductor. *Phys. Rev. Lett.* DOI: 10.1103/PhysRevLett.105.136805 (2010).
15. Splendiani, A. *et al.* Emerging photoluminescence in monolayer MoS₂. *Nano Lett.* **10**, 1271–1275 (2010).
16. Fivaz, R. & Mooser, E. Mobility of charge carriers in semiconducting layer structures. *Phys. Rev.* **163**, 743–755 (1967).
17. Bertolazzi, S., Brivio, J. & Kis, A. Stretching and breaking of ultrathin MoS₂. *ACS Nano* **5**, 9703–9709 (2011).
18. Lee, H. S. *et al.* MoS₂ nanosheet phototransistors with thickness-modulated optical energy gap. *Nano Lett.* **12**, 3695–3700 (2012).
19. Yu, Y. *et al.* Controlled scalable synthesis of uniform, high-quality monolayer and few-layer MoS₂ films. *Sci. Rep.* DOI:10.1038/srep01866 (2013).
20. Zande, A. M. *et al.* Grains and grain boundaries in highly crystalline monolayer molybdenum disulfide. *Nat. Mater.* **12**, 554–561 (2013).
21. Conley, H. J. *et al.* Bandgap engineering of strained monolayer and bilayer MoS₂. *Nano Lett.* **13**, 3626–3630 (2013).
22. He, K., Poole, C., Mak, K. F. & Shan, J. Experimental demonstration of continuous electronic structure tuning via strain in atomically thin MoS₂. *Nano Lett.* **13**, 2931–2936 (2013).
23. Hui, Y. Y. *et al.* Exceptional tenability of band energy in a compressively strained trilayer MoS₂ sheet. *ACS Nano* **7**, 7126–7131 (2013).
24. Castellanos-Gomez, A. *et al.* Local strain engineering in atomically thin MoS₂. *Nano Lett.* **13**, 5361–5366 (2013).
25. Rice, C., Young, R. J., Zan, R. & Bangert, U. Raman-scattering measurements and first-principles calculations of strain-induced phonon shifts in monolayer MoS₂. *Phys. Rev. B* DOI:10.1103/PhysRevB.87.081307 (2013).
26. Kittel, C. *Introduction to Solid State Physics Ch.2*, 38–39 (John Wiley & Sons, Inc., New York London, 1968).
27. Liu, Y. *et al.* Layer-by-layer thinning of MoS₂ by plasma. *ACS Nano* **7**, 4202–4209 (2013).
28. Wang, X., Feng, H., Wu, Y. & Jiao, L. Controlled synthesis of highly crystalline MoS₂ flakes by chemical vapor deposition. *J. Am. Chem. Soc.* **135**, 5304–5307 (2013).
29. Kuc, A., Zibouche, N. & Heine, T. Influence of quantum confinement on the electronic structure of the transition metal sulfide TS₂. *Phys. Rev. B* DOI: 10.1103/PhysRevB.83.245213 (2011).
30. Mohiuddin, T. M. G. *et al.* Uniaxial strain in graphene by raman spectroscopy: G peak splitting, Grüneisen parameters, and sample orientation. *Phys. Rev. B* **79**, 205433–205440 (2009).
31. Ghosh, P. N. & Maiti, C. R. Interlayer force and Davydov splitting in 2H-MoS₂. *Phys. Rev. B* **28**, 2237–2239 (1983).
32. Molina-Sánchez, A. & Wirtz, L. Phonons in single-layer and few-layer MoS₂ and WS₂. *Phys. Rev. B* DOI: 10.1103/PhysRevB.84.155413 (2011).
33. Li, T. & Galli, G. Electronic properties of MoS₂ nanoparticles. *J. Phys. Chem. C* **111**, 16192–16196 (2007).
34. Lee, C. *et al.* Anomalous lattice vibrations of single and few layer MoS₂. *ACS Nano* **4**, 2695–2700 (2010).
35. Kuroda, N. & Nishina, Y. Davydov splitting of degenerate lattice modes in the layer compound GaS. *Phys. Rev. B* **19**, 1312–1315 (1979).
36. Scalise, E., Houssa, M., Pourtois, G., Afanas'ev, V. & Stesmans, A. Strain-induced semiconductor to metal transition in the two-dimensional honeycomb structure of MoS₂. *Nano Res.* **5**, 43–48 (2012).
37. Peelaers, H. & Van de Walle, C. G. Effects of strain on band structure and effective masses in MoS₂. *Phys. Rev. B* **86**, 241401–241405 (2012).
38. Lebègue, S. & Eriksson, O. Electronic structure of two-dimensional crystals from ab initio theory. *Phys. Rev. B* **79**, 115409–115412 (2009).
39. Tongay, S. *et al.* Thermally driven crossover from indirect toward direct bandgap in 2D semiconductors: MoSe₂ versus MoS₂. *Nano Lett.* **12**, 5576–5580 (2012).

Acknowledgments

This work was supported by National Natural Science Foundation of China (NSFC) (21373196), the Recruitment Program of Global Experts, the Fundamental Research Funds for the Central Universities (WK2060140014, WK2340000050), and a faculty start-up grant for S.A.D. at the University of California San Diego.

Author contributions

B.X. and J.Z. initiated the study. B.X. designed the experiments. L.Y., M.S. and S.Z. performed the experiments. X.C. and K.W. carried on theoretical calculations. B.X., J.Z., S.D. and L.F. analyzed the data. B.X., L.Y., J.Z., S.D. and L.F. prepared the manuscript. All the authors contributed to discussions of the project.



Additional information

Reprints and permission information is available online at <http://npg.nature.com/reprintsandpermissions/>

Supplementary information accompanies this paper at <http://www.nature.com/scientificreports>

Competing financial interests: The authors declare no competing financial interests.

How to cite this article: Yang, L. *et al.* Lattice strain effects on the optical properties of MoS₂ nanosheets. *Sci. Rep.* 4, 5649; DOI:10.1038/srep05649 (2014).



This work is licensed under a Creative Commons Attribution-NonCommercial-NoDerivs 4.0 International License. The images or other third party material in this article are included in the article's Creative Commons license, unless indicated otherwise in the credit line; if the material is not included under the Creative Commons license, users will need to obtain permission from the license holder in order to reproduce the material. To view a copy of this license, visit <http://creativecommons.org/licenses/by-nc-nd/4.0/>